

JGR Atmospheres



RESEARCH ARTICLE

10.1029/2023JD040429

Key Points:

- Two similar SST patterns belie two different mechanisms forcing the subtropical high's westward extensions
- Tropical Pacific SST gradient forcing of westward extensions can be suppressed by its extratropical SST forcing
- Remote Atlantic SST forcing drives westward extensions when the local net Pacific forcing is weak

Supporting Information:

Supporting Information may be found in the online version of this article.

Correspondence to:

J. J. Jones, jjpjones@purdue.edu

Citation:

Jones, J. J., Chavas, D. R., & Johnson, Z. F. (2024). Inter-basin versus intra-basin sea surface temperature forcing of the Western North Pacific subtropical high's westward extensions. *Journal of Geophysical Research: Atmospheres*, 129, e2023JD040429. https://doi.org/10.1029/2023JD040429

Received 17 NOV 2023 Accepted 22 JUL 2024

Author Contributions:

Conceptualization: Jhordanne J. Jones, Daniel R. Chavas, Zachary F. Johnson Formal analysis: Jhordanne J. Jones Funding acquisition: Daniel R. Chavas Methodology: Jhordanne J. Jones, Daniel R. Chavas

Supervision: Daniel R. Chavas Visualization: Jhordanne J. Jones, Daniel R. Chavas

Writing – original draft: Jhordanne J. Jones

Writing – review & editing: Jhordanne J. Jones, Daniel R. Chavas, Zachary F. Johnson

© 2024. The Author(s).

This is an open access article under the terms of the Creative Commons Attribution-NonCommercial-NoDerivs License, which permits use and distribution in any medium, provided the original work is properly cited, the use is non-commercial and no modifications or adaptations are made.

Inter-Basin Versus Intra-Basin Sea Surface Temperature Forcing of the Western North Pacific Subtropical High's Westward Extensions

Jhordanne J. Jones^{1,2}, Daniel R. Chavas², and Zachary F. Johnson³

¹University Corporation for Atmospheric Research, Boulder, CO, USA, ²Department of Earth, Atmospheric, and Planetary Sciences, Purdue University, West Lafayette, IN, USA, ³Department of Earth and Atmospheric Science, Central Michigan University, Mount Pleasant, MI, USA

Abstract Zonal extensions of the Western Pacific subtropical high (WPSH) strongly modulate extreme rainfall activity and tropical cyclone (TC) landfall over the Western North Pacific (WNP) region. These zonal extensions are primarily forced on seasonal timescales by inter-basin zonal sea surface temperature (SST) gradients. However, despite the presence of large-scale zonal SST gradients, the WPSH response to SSTs varies from year to year. In this study, we force the atmosphere-only NCAR Community Earth System Model version 2 simulations with two real-world SST patterns, both featuring the large-scale zonal SST gradient characteristic of decaying El Niño-developing La Niña summers. For each of these patterns, we performed four experimental sets that tested the relative contributions of the tropical Indian Ocean, Pacific, and Atlantic basin SSTs to simulated westward extensions over the WNP during June-August. Our results indicate that the subtle differences between the two SST anomaly patterns belie two different mechanisms forcing the WPSH's westward extensions. In one SST anomaly pattern, extratropical North Pacific SST forcing suppresses the tropical Pacific zonal SST gradient forcing, resulting in tropical Atlantic and Indian Ocean SSTs being the dominant driver. The second SST anomaly pattern drives a similar westward extension as the first pattern, but the underlying SST gradient driving the WPSH points to intra-basin forcing mechanisms originating in the Pacific. The results of this study have implications for understanding and predicting the impact of the WPSH's zonal variability on tropical cyclones and extreme rainfall over the WNP.

Plain Language Summary Westward extensions of the Western North Pacific subtropical high (WPSH) drive rainfall extremes over the Western North Pacific basin, and is important for the prediction of summer rainfall, including monsoonal rainfall and tropical cyclone activity. Studies have previously highlighted the importance of tropical large-scale zonal sea surface temperature (SST) gradient—warm tropical Indian Ocean in conjunction with cold equatorial eastern Pacific Ocean—in developing and maintaining the summer WPSH and westward extensions. Here, we further show that even with very similar SST patterns, the large-scale zonal SST pattern may belie forcing from inter-basin SSTs versus intra-basin SSTs. We find that the net influence from the Pacific basin determines whether inter-basin remote SST gradients versus intra-basin Pacific SST gradients are the predominant driver of westward extensions.

1. Introduction

The zonal variability of the Western Pacific subtropical high (WPSH) significantly influences weather and climate across the Western North Pacific (WNP) region. It is a critical regional mechanism driving interannual boreal summer extreme rainfall variability over the Indo-Pacific region, including East Asian monsoon rainfall (Chang et al., 2000; Guan et al., 2019; B. Wang et al., 2013), Indian summer rainfall (Chaluvadi et al., 2021), and WNP tropical cyclone activity (Camp et al., 2018; Johnson et al., 2022; B. Wang et al., 2013; Q. Wu et al., 2020). Many statistical and dynamical models include the WPSH's zonal variability as a source of predictability (Kosaka et al., 2013; B. Wang et al., 2013) and provide skillful dynamical predictions of TC landfall risk across the WNP (Camp et al., 2018; Johnson et al., 2022). Therefore, improving our understanding of what drives the WPSH's zonal variability is crucial for accurately predicting regional extreme precipitation events.

Differential heating underpins the summer subtropical anticyclones' strengthening, maintenance, and overall variability in multiple ways. Monsoonal latent release over land shifts diabatic heating northward and induces subsidence eastward of the anomalous heating (Hoskins, 1996; Rodwell & Hoskins, 2001). This subsidence

JONES ET AL. 1 of 15

21698996, 2024, 15, Downloaded from https://agupubs.onlinelibrary.wiley.com/doi/10.1029/2023JD040429, Wiley Online Library on [27/05/2025]. See the Terms and Conditions (https://onlinelibrary.wiley

drives equatorward flow and cooler SSTs along the eastern boundary of the subtropical oceanic basins, which drives further subsidence over the subtropics. Meanwhile, condensational latent heating and land-sea diabatic heating contrast warm SSTs to the west of the ocean basins, enhancing poleward flow along the western boundary (P. Chen et al., 2001; Liu et al., 2004; Miyasaka & Nakamura, 2005; Yimin & Guoxiong, 2004) and yielding the characteristic asymmetric SST pattern associated with the summer anticyclones (Seager et al., 2003).

Pacific-basin SST variability drives much of the WPSH's interannual variability. During the mature El Niño winter, El Niño's decay and the seasonal warming in the tropical Indian Ocean (TIO) and WNP result in anticyclonic flow over the WNP via Kelvin wave response (T. Li et al., 2017; B. Wang et al., 2003; B. Wu et al., 2009). The enhanced easterlies further support El Niño decay. Therefore, summers with an enhanced WPSH westward extension, characterized by anomalous positive geopotential heights and anticyclonic flow over the WNP, tend to be El Niño-decaying, La Niña-developing or La Niña-persisting summers (Jong et al., 2020; Kosaka et al., 2013; Stuecker et al., 2015). From June to August (JJA), zonal SST gradients between the tropical Indian Ocean, WNP, Central Pacific (CP), and Eastern Pacific (EP) domains maintain the WPSH. B. Wang et al. (2013) identified two distinct SST gradient patterns accounting for approximately 53% of the WPSH's variability. The first mode showed positive TIO SST and negative WNP SST anomalies, associated with positive feedback between the WPSH and the zonal SST gradient and a decaying El Niño in the EP region. The second mode showed positive WNP SST and negative CP and EP SST anomalies associated with a developing/persisting La Niña. The WPSH is also remotely forced by North Atlantic SSTs. Tropical North Atlantic warming drives increased large-scale ascent over the Atlantic and Indian Oceans, resulting in stronger descent in the Central and Eastern Pacific basins (Hong et al., 2014, 2015; Rong et al., 2010; Zhou et al., 2009).

Additionally, the WPSH is a combined response to the relative contributions from local and remote SST forcing, which change as the seasons progress (Z. Chen et al., 2016; B. Wu et al., 2010). Xie et al. (2009) used atmosphere-only global climate model (GCM) experiments to show that the TIO warming's spatial distribution and magnitude impacted the WPSH's intensity. Forcing an atmosphere-only GCM with observed SSTs, B. Wu et al. (2010) and Z. Chen et al. (2016) later showed that the remote forcing of a cool WNP complemented the warm TIO in forcing the WPSH during the El Niño-decaying summer. H. Li et al. (2020) used the Community Atmospheric Model version 5 to force July–September westward extensions with observed SSTs in the wider tropical belt between 20°S and 20°N, which were further restrained to the TIO, tropical Pacific, and tropical Atlantic forcing regions. They found that the westward extensions were driven predominantly by the tropical ocean regions, particularly the TIO. The convective heating over the TIO triggers eastward-propagating baroclinic Kelvin waves that strengthen the anomalous anticyclone and suppress precipitation over the WNP. Note that H. Li et al. (2020)'s summer SST forcing pattern reflects a La Niña Modoki pattern, which has simultaneously warm TIO, EP, and Atlantic regions but a cool WNP region.

Recent studies have pointed out that the winter El Niño's magnitude and summer El Niño's decay rate also influence the summer WPSH's intensity and westward extensions. Slower El Niño decay rates result in a weaker summer westward extension, while faster El Niño decay rates result in deeper westward extensions (W. Chen et al., 2012; Z. Chen et al., 2016; W. Jiang et al., 2019; L. Jiang et al., 2023; M. Wu et al., 2020). W. Chen et al. (2012) found that the peak winter El Niño's decay rate is related to TIO warming. Anomalous equatorial easterly flow triggered by winter TIO warming strengthens during the spring for fast-decaying El Niño seasons, extending the easterlies to the CP region and speeding up El Niño's decay. The enhanced easterlies and faster El Niño decay promote and maintain the WNP anomalous anticyclone and westward extensions that the developing La Niña later maintains. For slow-decaying El Niños, less intense TIO warming promotes weaker easterlies in the CP, resulting in slower El Niño decay and weaker anticyclonic flow over the WNP. The WPSH's sensitivity to El Niño transition results in large uncertainties in simulations and future projections of WPSH in a warmer climate (M. Wu et al., 2020, 2021).

These studies show that the WPSH westward extensions are highly sensitive to SST variability in multiple regions. Differing from H. Li et al. (2020) and L. Jiang et al. (2023), our study deconstructs two global SST forcing patterns (hereafter, known as COMP1 and COMP2) with similar El Niño decay rates and compares their impact on WPSH westward extensions. We find that while the WPSH's westward extension response to the SST forcings differ in the way expected (as described above), the relative contributions from the underlying regional SST forcings differ greatly suggesting different mechanisms driving atmospheric response over the WNP. The mechanisms that have been revealed are categorized as inter-basin versus intra-basin SST forcing. Here, we

JONES ET AL. 2 of 15

define inter-basin forcing as the remote impact of an external ocean on atmospheric climate over the Pacific basin; intra-basin describes how local Pacific SSTs influence atmospheric conditions within the same basin. We quantify and examine the WPSH's response to regional and sub-regional SST contributions in each case. Our science questions for this study are as follows.

- 1. Are large-scale SST patterns with similar El Niño-decay rates driven by the same underlying mechanism?
- 2. Which regional SST differences promote an inter-basin versus intra-basin mechanism?
- 3. How do the roles of the tropical Indian Ocean SSTs, equatorial central and eastern Pacific SSTs, and North Atlantic Ocean SSTs vary in an inter-basin versus intra-basin SST forcing?

The paper is outlined as follows. In Section 2, we describe the data, methods, and experimental setup. Section 3 provides an observational analysis of the two similar SST patterns and their impact on the WPSH and its westward extensions. Section 4 outlines the results of our SST forcing experiments. Section 5 gives the discussion and conclusions.

2. Data and Methods

2.1. Data

Monthly variable fields are sourced from the ECMWF fifth generation reanalysis (ERA5) data set (Hersbach et al., 2020). The ERA5 reanalysis data set has a horizontal grid resolution of 31 km with 137 vertical levels, and provides data from 1 January 1940 to the present. Variables with a $0.25^{\circ} \times 0.25^{\circ}$ grid resolution were obtained from the Copernicus Climate Data Store (https://cds.climate.copernicus.eu/cdsapp#!/home) and are as follows: 850-hPa geopotential heights (Z850), 250-hPa, and 850-hPa zonal and meridional winds (UV250, UV850), and sea surface temperatures (SSTs). We analyze these fields over the time period 1979–2019. Anomalies calculated from these fields are relative to the 1979–2019 mean climatology. Note that our anomaly fields have not been detrended. In Section 3, we use the reanalysis variable fields to examine and characterize anomaly composites associated with the WPSH's extensions.

The WPSH's intensity and westward extensions are determined using the Z850 anomaly field. There are a variety of ways in which WPSH variability may be defined. Common indices used are calculated with geopotential height anomalies at 850-hPa (Camp et al., 2018; B. Wang et al., 2013) and 500-hPa (H. Li et al., 2020; Qian & Shi, 2017; Zhou et al., 2009). Less commonly used indices include 850-hPa relative vorticity (Kosaka et al., 2013; X. Wang et al., 2021). Following B. Wang et al. (2013), Camp et al. (2018), and Johnson et al. (2022), we define the WPSH intensity using 850-hPa geopotential height anomalies averaged over the tropical WNP region (10°-30°N, 100°E–180°). The westward extension index (WEI) is generally defined as the most westward longitude reached along a specified contour within the WNP region. Dong and He (2020) and H. Li et al. (2020) use similar methods to characterize the WPSH's zonal extensions in the 500-hPa height fields. However, with background warming, positive geopotential height anomalies spread across the WNP due to atmospheric expansion, giving the illusion that the Pacific STH extends westward when measured by the spatial extent of a given height (He & Zhou, 2015; L. Wu & Wang, 2015; Zhou et al., 2009). To account for this, the WPSH index, from which we choose the COMP1 and COMP2 composite years, is detrended. In the simulations to follow, we employ the measure suggested by Yan-Yan and Xiao-Fan (2015) and He and Zhou (2015). The WPSH's westernmost longitude is defined by the location of the 0-m contour in the 850-hPa eddy geopotential height field with the 0°-40°N zonal mean removed.

The SST fields are used to calculate monthly standardized anomalies for the tropical Indian Ocean (TIO, 30°S–30°N, 40°–120°E), WNP, tropical North Atlantic (0°–20°N, 100°W–0°) and El Niño Southern Oscillation (ENSO) SST variability. The conventional Niño-3.4 region has been extended to 160°E to better capture nonlinear seasonal cold-tongue SST variations in the Central Pacific and equatorial eastern Pacific, as proposed by Williams and Patricola (2018). Therefore, the acronym ENSO is used hereafter to refer to the deep tropical equatorial Pacific SST anomalies between 10°S–10°N and 160°E–120°W.

2.2. The COMP1 and COMP2 SST Patterns

Figure 1 shows the SST, Z850, and Z850 anomaly fields associated with the two SST pattern composites we examine in this study. The first SST composite (COMP1) comprise years 1980, 1995, 1998, 2003, and 2010, in which the detrended June–August WPSH is most enhanced. COMP1 features positive anomalies in the TIO,

JONES ET AL. 3 of 15

21698996, 2024, 15, Downloaded from https://agupubs.onlinelibrary.wiley.com/doi/10.1029/2023JD040429, Wiley Online Library on [27/05/2025]. See the Terms and Conditions (https://online

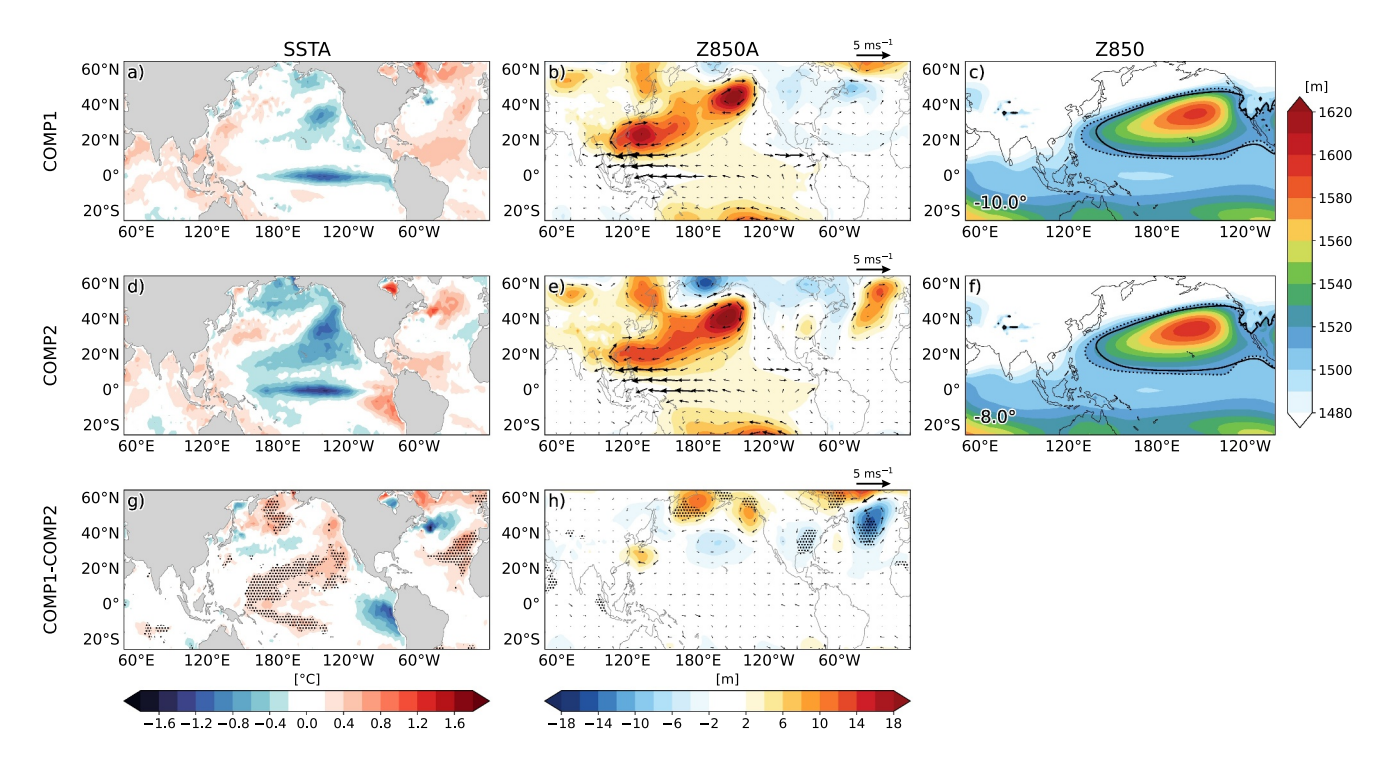


Figure 1. Composites and composite difference of June–August mean (a, d, g) SST anomalies and (b, e, h) Z850 anomalies (shaded contours, m) with horizontal winds (quivers, m s⁻¹), and (c, f) mean Z850 fields and 0-m eddy geopotential contours comparing the composites (dotted contour) and climatology (solid contour) for COMP1 (1998, 2010, 1980, 1995, and 2003) and COMP2 (1980, 1983, 1998, 1999, and 2010). Hatching highlight composite differences that are statistically significant at the 90% confidence level based on the Wilcoxon signed-rank test for N = 5. The longitudinal extent (relative to climatology) is given in the lower left corner in (c, f).

WNP, and ATL region with negative anomalies in the central and equatorial eastern Pacific regions that is characteristic of El Niño-decaying summers (Figure 1a). This SST pattern is associated with anomalous positive geopotential height anomalies and anticyclonic flow over the WNP which extends the WPSH further west (Figures 1b and 1c). The second SST forcing (COMP2) is composited from years 1980, 1983, 1998, 1999, and 2010, and is an alteration to the COMP1 SST composite. Like COMP1, COMP2 also features TIO, WNP, and ATL warming but widespread cooling across the central and equatorial eastern Pacific regions (Figure 1d). COMP2 also produces positive geopotential height anomalies and anticyclonic flow over the WNP, resulting in a similar westward extension (Figures 1e and 1f).

While there is considerable overlap between the two sets of years, the addition of 1983 and 1999 in COMP2 results in a larger spread of negative SST anomalies across the central and eastern Pacific regions akin to a more developed La Niña pattern (Figure 1d). This partial overlap is by design. As we will show below, differences in SST anomaly patterns between the two composites result in markedly different outcomes for the drivers of the westward extension. In practice, experiments for these two distinct composites were initially done by accident, but serendipitously, they yielded an interesting contrast in behavior that became the focus of this work.

Figure 1g indicate that most of the differences in SSTs between COMP1 and COMP2 lie in the tropical and subtropical central and eastern Pacific, and the subtropical/extratropical Atlantic regions. These differences are statistically significant at the 90% confidence level. But the Z850 anomaly composite difference shows little significant change over the WNP and westward extensions (Figure 1h). The two SST composites also show similarities in the monthly evolution of SSTs in key regions for WPSH development and maintenance. Figures 2a and 2b show the YR(-1) and YR(0) monthly mean standardized anomalies averaged over the TIO, extended ENSO domain (20°S–20°N, 160°E–120°W), WNP, and the TNA. COMP1's D(-1)JF El Niño event is slightly stronger than that of COMP2, but both composites indicate a comparable rate of decay of the winter El Niño. The June–August La Niña SST signal averages –0.66°C for COMP1 and –0.78°C for COMP2. The observed COMP1 and COMP2 precipitation anomalies (Figure S1 in Supporting Information S1) show that the two SST patterns very similar diabatic heating patterns with COMP2 having stronger heating in the subtropical WNP.

JONES ET AL. 4 of 15

21698996, 2024, 15, Downloaded from https://agupubs.onlinelibrary.wiley.com/doi/10.1029/2023JD040429, Wiley Online Library on [27/05/2025]. See the Terms and Conditions (https://onlinelibrary.wiley.com/term

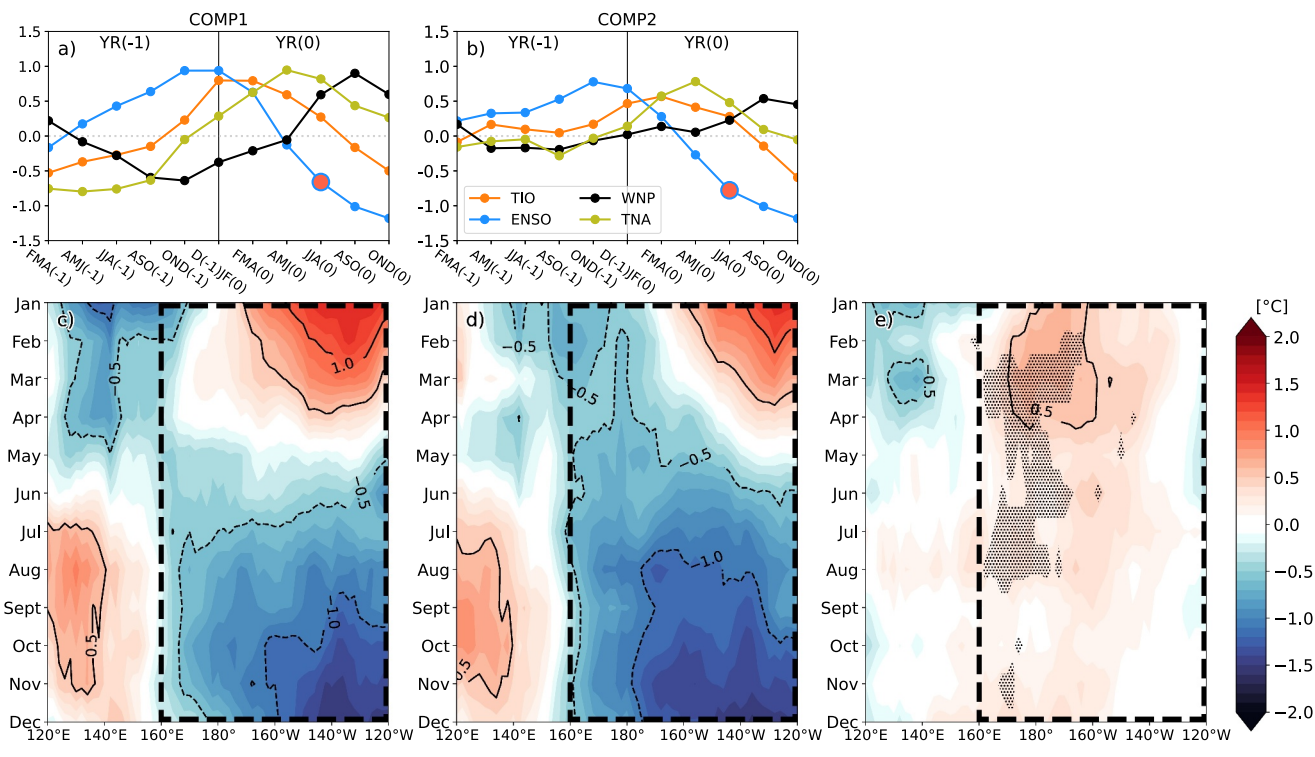


Figure 2. (a, b) Seasonal standardized SSTs averaged over the TIO, WNP, equatorial eastern Pacific (ENSO), and the tropical North Atlantic (TNA) regions for the contemporaneous year (YR(0)) and the preceding year (YR(-1)). The YR(0) June–August (JJA) is highlighted by the pink dot. ENSO values during JJA are highlighted by the large pink dots. (c, d) Time-longitude plot averaged over 20° S– 20° N illustrates ENSO's monthly evolution during YR(0) and (e) the time-longitude composite difference. Dashed box outlines the ENSO region, defined as 20° S– 20° N and 160° E– 120° W. The extended ENSO domain considers the longitudinal extent of the cold tongue anomalies (Williams & Patricola, 2018). The TNA region is defined as 0° – 20° N, 100° W– 0° . Hatching indicates statistical significance at the 90% confidence level based on the Wilcoxon signed-rank test for N = 5.

Figures 2c and 2d illustrate the monthly evolution of standardized SST anomalies averaged over the Pacific tropical band between 20°S–20°N and 120°E–120°W. The composite difference is given in Figure 2e. The figures indicate that both COMP1 and COMP2 reflect an eastern Pacific (EP) La Niña-type signal, and even have a similar seasonal development of La Niña, following from a strong winter EP El Niño from the preceding year (Figures 2a and 2b). The key difference between the two composites lies in the decay of the winter El Niño. In COMP1, the eastward migration of central Pacific negative SST anomalies doesn't occur until around April–May. In contrast, for COMP2, this eastward migration begins the year before (not shown) and can be observed in months January–March. In consequence of the earlier decay of COMP2's winter El Niño, negative SSTs >0.5°C develop earlier in the summer, and are shown to spread further west into the central Pacific region.

2.3. CAM6 and Experiment Setup

We simulate the response of the WPSH using the atmosphere-only component of Community Earth System Model version 2.2.0 (CESM2). The Community Atmosphere Model version 6 (CAM6) uses a $0.9^{\circ} \times 1.25^{\circ}$ horizontal resolution and 32 vertical levels with a Finite Volume (FV) dynamical core (Danabasoglu et al., 2020). Our experimental setup consists of atmosphere-only (AMIP) simulations using the F2000CLIMO configuration driven by a historical 12-monthly SST climatology representative of present-day climate, and is run with active atmosphere (CAM6) and land (CLM5) components. A detailed description of F2000CLIMO and other CESM2 run configurations can be found at https://www.cesm.ucar.edu/models/cesm2/config/compsets.html. The F2000CLIMO compset provides a simplified experimental setup that directly tests the general circulation's response to recurring seasonal SST changes independent of year-to-year SST variability.

To examine how SSTs force the WPSH, we run the F2000CLIMO component set that forces CAM6 with a 12-month prescribed SST climatology. The control experiment (CTRL) is taken to be the 1979–2019, calculated from the ERA5 reanalysis data set. Note that the ERA5 SST fields are regridded to the CAM6 grid resolution

JONES ET AL. 5 of 15



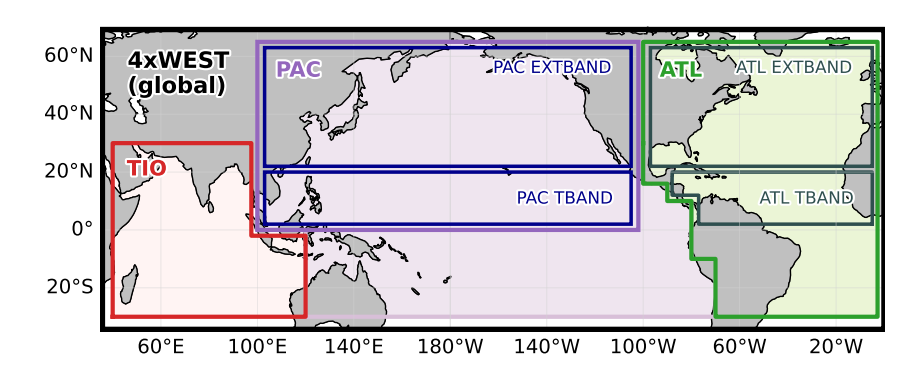


Figure 3. Outline of the main SST pattern forcing domains. The main domains include the tropical Indian Ocean (TIO, red), the North Pacific Ocean basin (PAC, purple), and the Atlantic Ocean basin (ATL, green).

 $(1.9^{\circ} \times 2.5^{\circ})$, and are linearly interpolated to fill in masked land values prior to running the simulations. Then, the COMP1 and COMP2 SST patterns are quadrupled in magnitude (4xWEST) to enhance the westward extension signal in the simulations relative to the CTRL simulation. The simulations are allowed to run for 6 years. The first year is thrown out to account for model initialization, and the atmospheric response is averaged over years 2–6. We ran initial experiments out to years 6, 11, 16, and 31 and found no significant changes from the simulated westward extent averaged over years 2–6. Note that, since the simulations are driven only by the prescribed 12-month SST climatology, the simulations are not forced by SST variations from preceding years, and therefore, doesn't take into account lagged air-ocean impacts, for example, ENSO's and TIO's lagged relationships from the year prior (M. Chen et al., 2019). Similarly, the WPSH is also a result of coupled air-sea interactions (T. Li et al., 2017). The study to follow only examines the atmospheric response to the prescribed SSTs. In the sections to follow, we compare the WPSH's response across the 4xWEST simulations.

To test which specific regional SST anomalies generate an enhanced WPSH comparable to the original 4xWEST simulations, we run a set of experiments in which we progressively constrain the region of SST anomalies included in the 4xWEST forcing. We note that, when forced with the WEST SST patterns, CAM6 produces a weaker westward extension relative to the CTRL experiment (not shown). This suggests that tropical convection in CAM6 may be less effective in generating subtropical high responses, likely due to differences in the diabatic heating profiles (R. Chen et al., 2022). When the WEST SST pattern is doubled, there is a slight suppression of WNP precipitation (diabatic heating), but not enough to substantially improve westward extensions (Figure S2 in Supporting Information S1). As we quadruple the SST forcing (4xWEST), the diabatic heating over the Indo-Pacific is further reduced to allow for westward extensions comparable to the observed. Therefore, the 4xWEST forcing is chosen to enhance the simulated WPSH's westward extension relative to the control simulation, which produces a WPSH westward extension of 134.9°E and 128.7°E for COMP1 and COMP2, respectively. We illustrate this contribution by comparing the difference in the 850-hPa geopotential heights between the spatially adjusted experiments and the CTRL experiment. Figure 3 illustrates the forcing domains for the experiments listed in Table 1.

Table 1 lists and organizes all simulations analyzed in this study into four experimental sets. Excluding the *CTRL* and *4xWEST* experiments, all other experiments comprise constraining SST anomalies to select domains and zeroing SST forcing elsewhere. Experimental set 1 examines the individual contributions of the tropical Indian Ocean (TIO), Pacific Ocean (PAC), and Atlantic Ocean (ATL) basin SST anomalies to the global COMP1 and COMP2 *4xWEST* forcings. These three basins have previously been shown to play substantial roles in the development and maintenance of the WPSH (W. Li et al., 2012; T. Li et al., 2017; Lu & Dong, 2001; B. Wu et al., 2010). In the following sections, we will show that these basin contributions are not comparable between COMP1 and COMP2.

In experiment set 2, SSTs are constrained to the North Pacific basin (as defined in Table 1) and examines whether Pacific SST magnitude, and consequently the strength of the zonal SST gradient across the Pacific, drives the stark difference in response between the COMP1 *PAC* and COMP2 *PAC* forcings. For these experiments, the magnitude of negative *PAC* SST anomalies (-SSTA) for COMP1 is doubled (*PACx2*) and then tripled (*PACx3*) to

JONES ET AL. 6 of 15

Table 1
List of Sea Surface Temperature Forcing Experiment Sets, Regional Domains Used, and Brief Descriptions of Each Experiment

Experiment set	Experiment name	Description
1	1979–2019 Control (CTRL)	-
	4xWEST (Global)	_
	4xWEST minus ATL	ATL basin SSTs zeroed
	4xWEST minus ATL, TIO	Both ATL and TIO basin SSTs zeroed
2	North Pacific basin (PAC)	COMP1, COMP2 experiments
	PACx2	COMP1 PAC -SSTA multiplied by 2, with lingering El Niño + SSTA changed to -SSTA
	PACx3	As for PACx2, but -SSTA multiplied by 3
3	PAC TBAND	0°–20°N, 100°E–100°W
	PAC EXTBAND	20°–60°N, 100°E–100°W
4	ATL only	North and South Atlantic basins
	ATL TBAND	$0^{\circ}-20^{\circ}N$, $100^{\circ}W-0^{\circ}$
	ATL EXTBAND	20°–60°N, 100°W–0°

enhance the original COMP1 *PAC* zonal SST gradient. Note that the *PACx2* and *PACx3* are conducted only for COMP1's *PAC* forcing.

Experiment sets 3 and 4 examine the individual contributions of intra-basin SST forcing by constraining SSTs to the tropical (*TBAND*) and extratropical (*EXTBAND*) domains in the North Pacific and Atlantic basins, respectively. The TBAND and EXTBAND domains were chosen based on the distribution of COMP1 minus COMP2 SST differences (Figure 3c). Additionally, L. Jiang et al. (2023) showed that the subtropical and extratropical regions may provide additional forcing along with well-known forcing from the Pacific and Atlantic tropical belts. Therefore, we define *PAC TBAND* and *PAC EXTBAND* intra-basin SST forcings for the North Pacific basin, and *ATL TBAND* and *ATL EXTBAND* SST forcings for the Atlantic basin.

For all experiments, the change in WEI is taken relative to the mean control. Statistical significance is determined via sample mean bootstrapping for a sample size of N = 5. Therefore, extensions westward of 135.8°E are considered statistically significant at the 95% level for 4xWEST simulations. Note also that no smoothing was applied to the edges of the SST patterns. A comparison of the SST-forced simulations with smoothing versus no smoothing achieved similar results (not shown). Finally, we acknowledge that the WPSH is maintained by coupled atmosphere-ocean interactions (Seager et al., 2003). By using atmosphere-only simulations, our paper focuses only on the atmosphere's response to the SST pattern.

3. Two Similar SST Patterns Belie Two Different SST Forcing Mechanisms

In the CAM6 simulations, COMP1 and COMP2 show comparably strong westward extensions. Figures 4a and 4b illustrate the atmospheric response in 850-hPa geopotential heights to the *4xWEST* global SST forcing for COMP1 (Figure 4a) and COMP2 (Figure 4b). COMP1 and COMP2 produce WEI changes of -17° and -23°, respectively, statistically significant at the 95% confidence level from the *CTRL*. The two SST patterns also produce anomalous anticyclones of similar intensity over the WNP (not shown). This result is consistent with our observational analysis (Figures 2 and 3) and shows that COMP1 and COMP2 have similar impacts on the WPSH.

Despite similar responses to global SST anomalies, experiments constraining SST anomalies to individual basins give very different results, suggesting different sources of forcing. The first experimental set examines the relative contributions of three key regions for westward extensions simulated by the 4xWEST experiments: the ATL, TIO, and PAC. Figures 4c and 4d illustrate the COMP1 and COMP2 4xWEST minus ATL experiments, respectively, that illustrate the impact of removing ATL SSTs from the global SST forcing pattern. Figures 4e and 4f show the result of further removing TIO SSTs from the global SST forcing pattern, leaving just the PAC basins. Note that the westward extensions produced by COMP1 4xWEST fall off quickly once the ATL (and, to a lesser extent, the TIO) is removed. In contrast, for the COMP2 4xWEST simulations, the PAC SSTs maintain the westward extension observed for its 4xWEST simulation, with only a small change in WEI with the removal of TIO. This

JONES ET AL. 7 of 15

21698996, 2024, 15, Downloaded from https://agupubs.onlinelibrary.wiley.com/doi/10.1029/2023JD040429, Wiley Online Library on [27/05/2025]. See the Terms and Conditions (https://onlinelibrary.wiley.com/terms

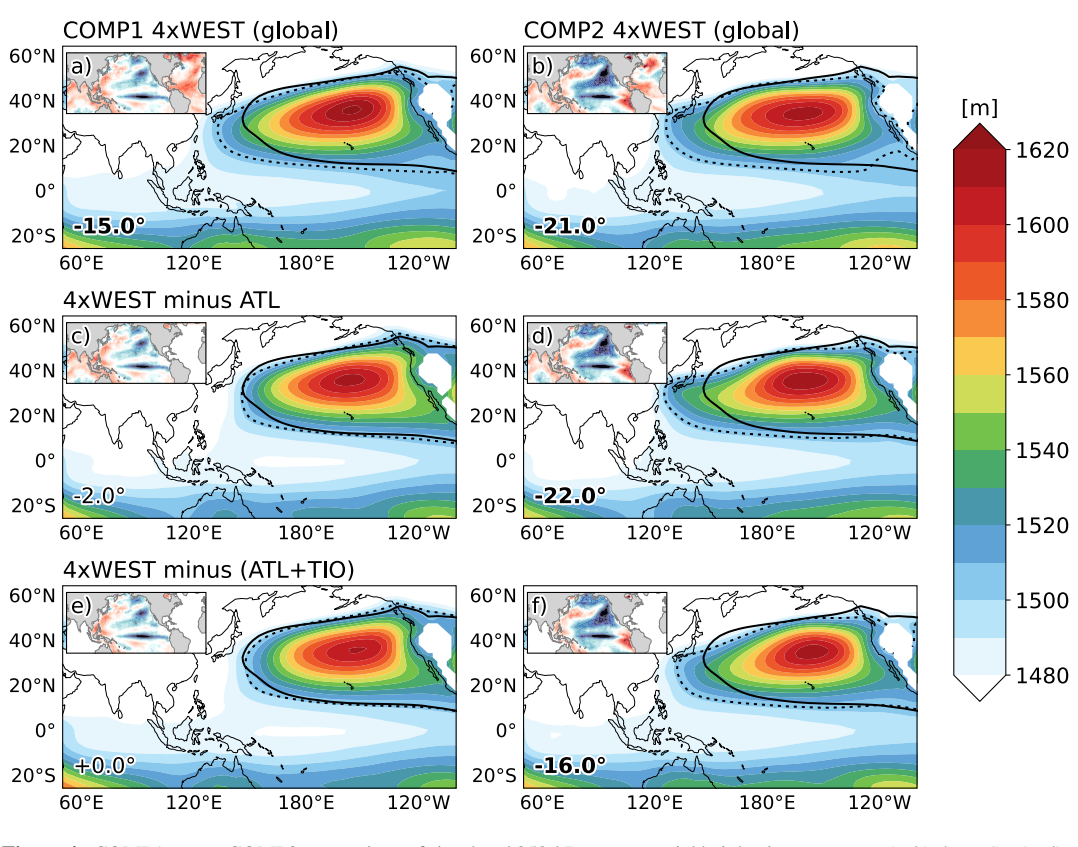


Figure 4. COMP1 versus COMP2 comparison of simulated 850-hPa geopotential heights in response to (a, b) 4xWEST, (c, d) 4xWEST minus ATL, (e, f) 4xWEST minus ATL + TIO simulations. Inset plots showcase the respective SST forcing for each simulation. The solid black contour outlines the 1,510-gph contour in CTRL simulation, while dashed contours outline the 1,510-gph contour for the respective forcing simulations. The mean westward extent index (WEI) value produced by each experiment, expressed as the change relative to the CTRL WEI, is given in the bottom left corner of each subplot. Note that negative (positive) WEI changes indicate a westward extension (eastward retraction). WEI changes that are statistically significant at the 95% confidence level are highlighted in bold.

suggests that the COMP1 SST pattern forces westward extensions predominantly through inter-basin SST gradients, while the COMP2 SST pattern forces westward extensions through intra-basin Pacific SST gradients.

The large-scale SST pattern's forcing of westward extensions can be viewed from the perspective of the zonal Pacific overturning atmospheric circulation. Figures 5a and 5b illustrate the meridional cross-section of the tropical atmospheric circulation averaged from 0°–30°N. Both COMP1 and COMP2 are characterized by strong subsidence over the central Pacific (the descending arm of the Walker Circulation) and ascent over the TIO and Atlantic regions. In the lower levels, the strong easterly flow associated with an enhanced WPSH and westward extension may be observed over the Indo-Pacific/WNP region between 100°E–180°. As the ATL and TIO forcings are removed, the descending arm supporting the strong lower-level easterlies over the central Pacific collapses for COMP1 (Figures 5c and 5e) but remains intact for COMP2 (Figures 5d and 5f). Note that when SSTs are further constrained, the WNP proves to be the smallest region that has a statistically significant westward extension in COMP2. Therefore, for COMP1, the combined effect of the Atlantic SSTs and the tropical Pacific-Indian Ocean/WNP SST gradient leads to a robust westward extension of the STH.

So, why are the relative contributions of regional SSTs so different between the COMP1 and COMP2 SST patterns? From Figure 1c, we identify and examine three key regions of SST differences stand out in Figure 1c that may explain the difference in model response, which we further explore using the atmosphere-only CAM6 global climate model: the tropical and subtropical central and eastern Pacific SSTs, extratropical Pacific SSTs, and the subtropical and extratropical Atlantic SSTs.

JONES ET AL. 8 of 15

21698996, 2024, 15, Downloaded from https://agupubs.onlinelibrary.wiley.com/doi/10.1029/2023JD040429, Wiley Online Library on [27/05/2025]. See the Terms and Conditions (https://onlinelibrary.wiley

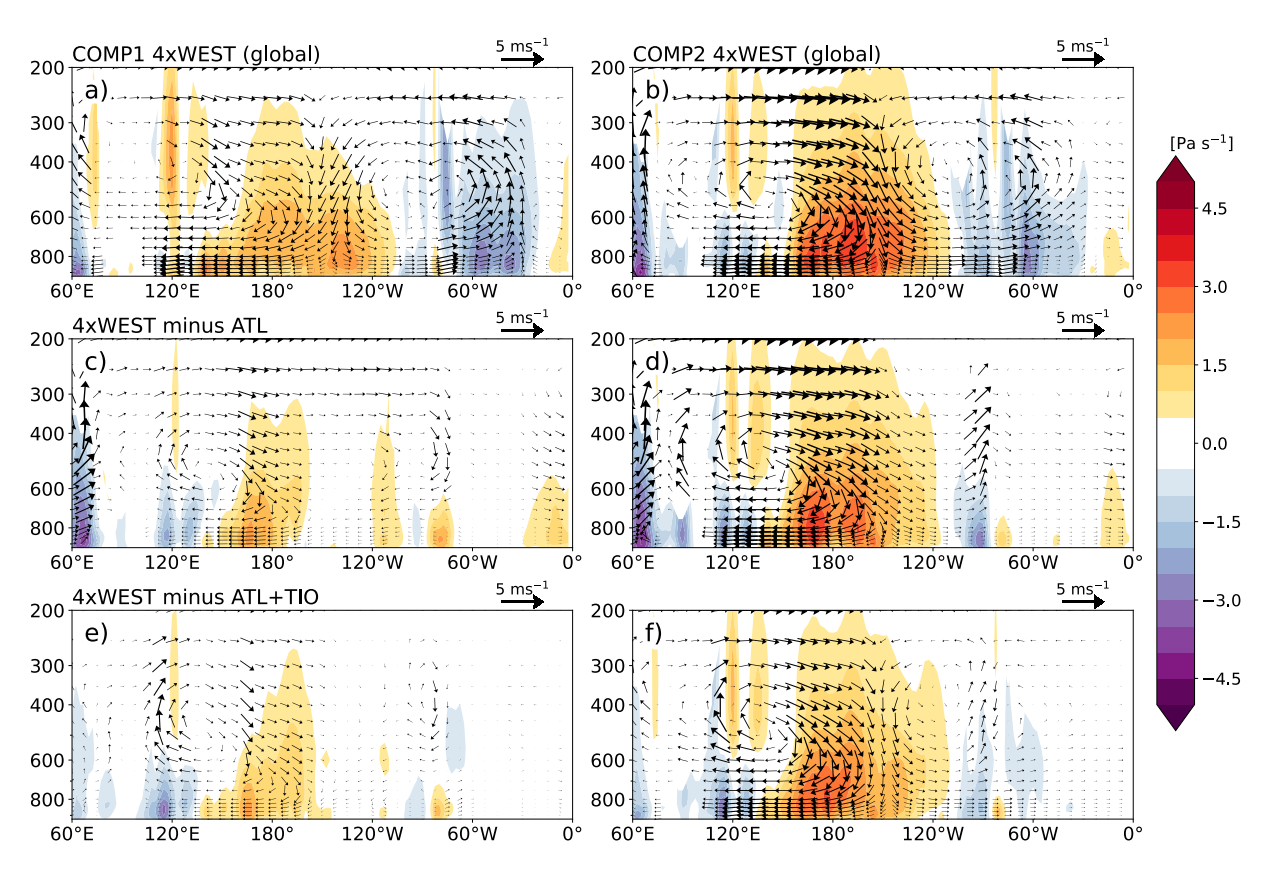


Figure 5. Meridionally averaged longitude-pressure plots of vertical velocity anomalies (shading), with quivers representing the magnitude and direction of scaled vertical ($\times 100$) and zonal ($\times 0.5$) wind anomalies from the same experiments as Figure 4. All plots are averaged over latitudes 0° – 20° N.

4. Tropical Pacific Intra-Basin SST Forcing of Westward Extensions Can Be Suppressed by Its Extratropical SST Forcing

Above, we showed that the relative contributions from remote SSTs (inter-basin forcing) predominantly drive westward extensions in COMP1 simulations, while local Pacific SSTs (intra-basin forcing) are the predominant driver in COMP2 simulations. L. Jiang et al. (2023) observed that the *TIO* and *ATL* SSTs were strong drivers of westward extensions in seasons with faster El Niño decays. The atmospheric response to the COMP1 SST pattern reflects the importance of remote SSTs to its forcing mechanism and is consistent with L. Jiang et al. (2023)'s findings (Figures 5a and 5e). But COMP2 contradicts the profile for this mechanism, despite having a stronger zonal SST gradient in the equatorial North Pacific than COMP1 with fairly similar El Niño decay rates (Figure 3). The results of this study and L. Jiang et al. (2023)'s results suggest that there is a big difference in the forcing impact between COMP1 and COMP2 Pacific basin SSTs. In the second experiment set, we test the differences between the COMP1 and COMP2 North Pacific SST forcing.

Figure 6 compares the simulated WPSH forced by North Pacific SST forcing (*PAC*) for COMP1 and COMP2. COMP1's *PAC* forcing produces a much weaker WPSH with an eastward retraction of +1° relative to *CTRL* (Figures 6a and 6e). In comparison, COMP2's *PAC* forcing produces a stronger WPSH and a relative westward extension of -16° (Figures 6d and 6h). From previous studies, it is expected that the more developed and more wide spread La Niña pattern in COMP2 may be creating a stronger zonal SST gradient and WNP anomalous anticyclone, and thus a stronger westward extension. To test whether the relatively weaker negative anomalies are the main reason for the weaker COMP1 *PAC* response, negative SST anomalies in COMP1's *PAC* forcing were doubled (*PACx2* in Figures 6b and 6f) and then tripled (*PACx3* in Figures 6c and 6g) to be comparable to COMP2's tropical SST gradient profile (see Figure S3 in Supporting Information S1).

Increasing the magnitude of the CP and EP negative anomalies results in only slightly improved yet statistically insignificant westward extensions (Figures 6a and 6b). Cooler SSTs in COMP1 PACx2 generate more subsidence

JONES ET AL. 9 of 15

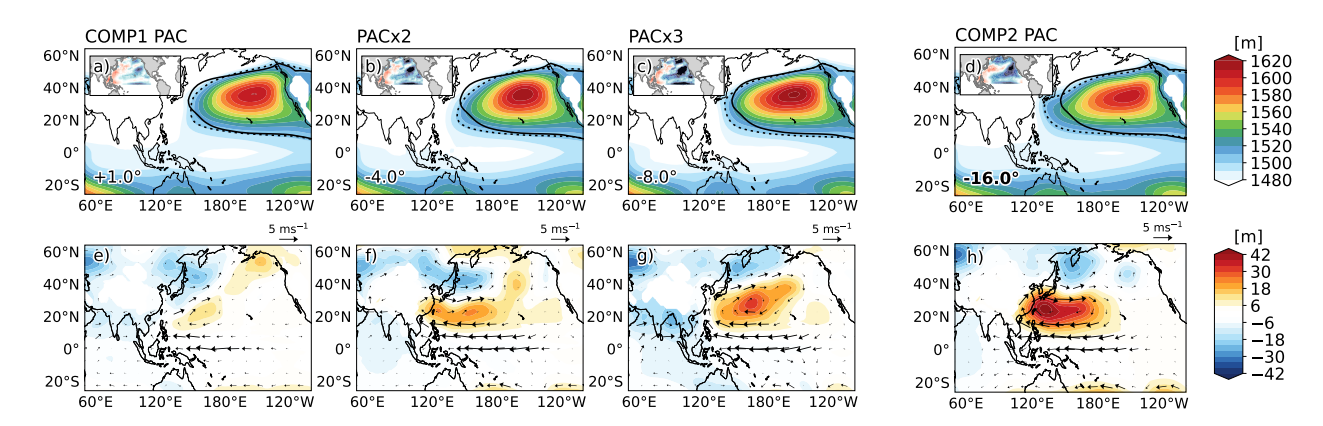


Figure 6. Simulation response in 850-hPa geopotential heights (top panels) and height anomalies relative to CTRL (bottom panels) to COMP1's (a, e) PAC, (b, f) PACx2, and (c, g) PACx3, compared to (d, h) COMP2's PAC experiment.

over the WNP that strengthens the WPSH and, thus, a stronger westward extension relative to COMP1 PAC. But any further cooling results in more intense precipitation over the Indo-Pacific region in response to increased WNP and CP subsidence (see the associated precipitation anomaly fields in Figure S4 in Supporting Information S1). Increased Indo-Pacific precipitation strengthens westerly monsoonal flow and negative Z850 anomalies over the TIO that restrict westward extensions in the COMP1 experiments (Figures 6e–6g).

Hence, the cooler CP and EP negative SST anomalies alone do not explain the stronger westward extension and anomalous anticyclone produced for the COMP2 *PAC* forcing (Figures 6d and 6h). There remains no significant westward shift in the presence of a substantial zonal SST gradient in the tropical Pacific (Figure S3 in Supporting Information S1). Therefore, in experimental set 3, we examine the contributions of SSTs in the Pacific tropical band (*TBAND*), between 0°–20°N, and subtropical and extratropical domain (*EXTBAND*) to the JJA westward extensions.

The SST anomalies from the Pacific tropical band alone produce a comparable westward extension in COMP1 and COMP2 (*PAC TBAND*; Figure 7a vs. Figure 7b). Similarly, the *PAC EXTBAND* forcings for both COMP1 and COMP2 produce negative Z850 anomalies and an anomalous cyclone over the WNP. However, the COMP1 *PAC EXTBAND* forces a stronger cyclonic flow, likely from the broader spread of positive SST anomalies along the western boundary. Similar observations have been made by L. Jiang et al. (2023). COMP1's *PAC EXTBAND* similarly produces an anomalous WNP cyclone, but the strength of this cyclone is curtailed by anomalous anticyclonic flow further north. Figure 7e shows the mean Z850 anomaly over the WNP for the *PAC TBAND* and *PAC EXTBAND*, and the net *TBAND* + *EXTBAND* forcing for both COMP1 and COMP2. For COMP1, the net *PAC* forcing reflects the suppression of the *PAC TBAND* forcing by *PAC EXTBAND* and produces similar Z850 anomalies as those forced by COMP1 *PAC* (Figure 5e). For COMP2, the relatively stronger forcing by COMP2 *TBAND* is enough to withstand forcing from its *EXTBAND*. Therefore, a key difference in the inter-basin versus intra-basin forcing of COMP1 and COMP2 stems from the difference in net Pacific forcing.

5. Remote Atlantic SST Forcing Drives Westward Extensions When the Local Net Pacific Forcing Is Weak

From experimental sets 2 and 3, we have shown that the net contributions between the *PAC* and *ATL* basin SSTs may vary depending on the net PAC forcing. When *PAC TBAND* is much stronger than *PAC EXTBAND*, the westward extensions are driven predominantly by intra-basin *PAC* SST forcing. When the *PAC TBAND* is suppressed by *PAC EXTBAND*, the *ATL* and *TIO* SSTs (and hence inter-basin SSTs) predominantly force the westward extensions. Since the *TIO* forcing for COMP1 and COMP2 are nearly identical (see Figure S5 in Supporting Information S1), the remaining SST difference lies with the *ATL*. So, are the *ATL* forcings significantly different between COMP1 and COMP2?

The results of the fourth experimental set show that the ATL SST forcing has comparable impacts on the WPSH's westward extension for both COMP1 and COMP2. Despite a clear difference between the COMP1 and COMP2 ATL SST patterns, both forcings produce similar WEI changes of -16° and -17° , respectively (Figures 8a and

JONES ET AL. 10 of 15

2169896, 2024, 15, Downloaded from https://agupub.son/inelibrary.wiley.com/doi/10.1029/2023JD404929, Wiley Online Library on [27/052025]. See the Terms and Conditions (https://onlinelibrary.wiley.com/terms-and-conditions) on Wiley Online Library for rules of use; OA articles are governed by the applicable Creative Commons Licensia

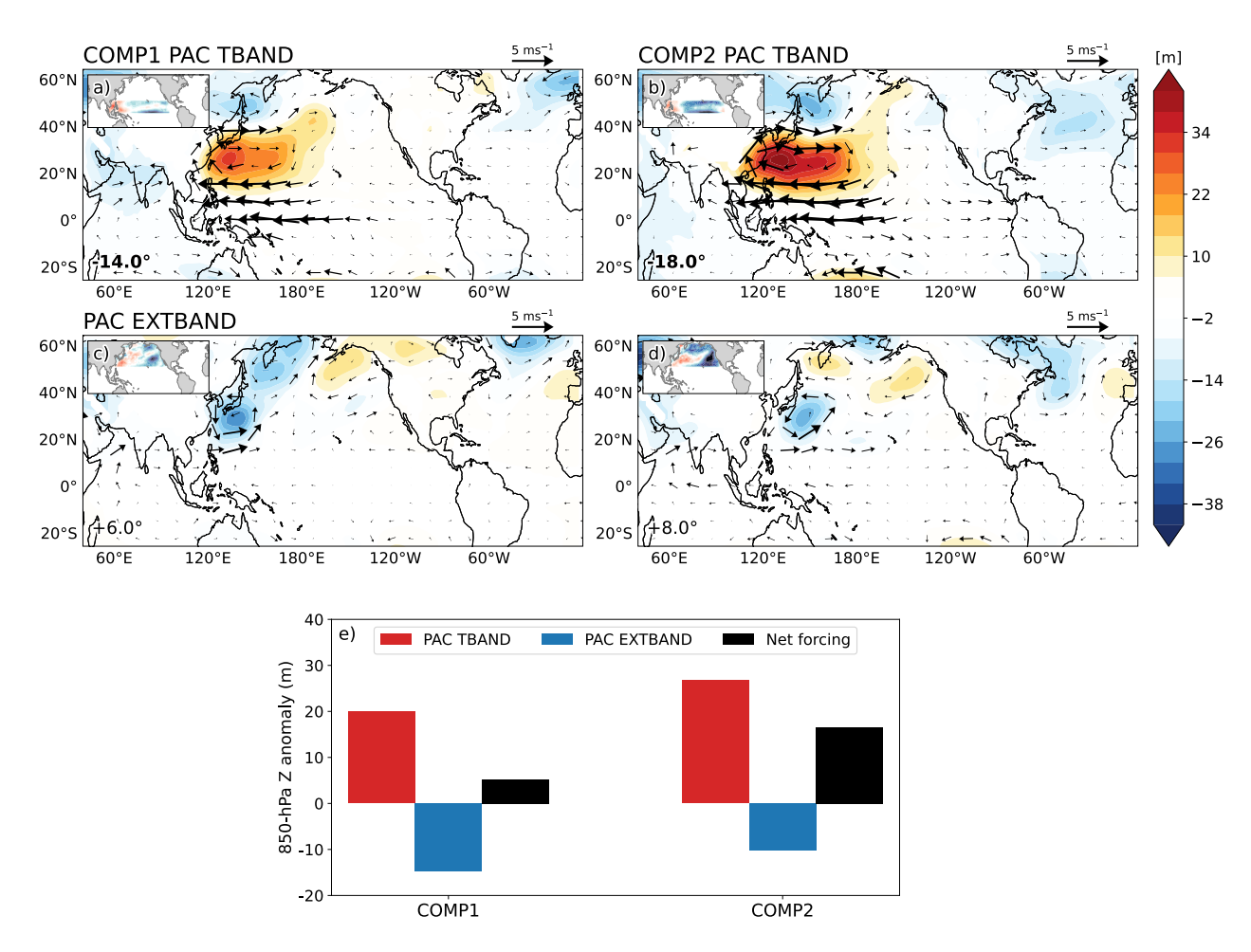


Figure 7. COMP1 versus COMP2 comparison of simulated 850-hPa geopotential height anomaly response to the forcing domains (a, b) *PAC TBAND*, and (c, d) *PAC EXTBAND*. (e) Mean 850-hPa geopotential anomaly averaged over 10°–30°N and 100°E–180° for COMP1's and COMP2's Pacific *TBAND* and *EXTBAND* simulations.

8b). The key mechanism underlying the Atlantic forcing of WNP westward extensions comprises the forcing of an anomalous low-level cyclonic circulation, strong westerlies, and negative Z850 anomalies over the western North Atlantic. This atmospheric response likely spurs strong ascent (see Figure 5a), which in turn forces strong subsidence over the WNP. When the *ATL* forcing is divided into the *ATL TBAND* and *ATL EXTBAND* domains, the *ATL TBAND* proves to be the key contributor to the larger *ATL* pattern (Figures 8c and 8d), consistent with studies that show that the tropical Atlantic SSTs can substantially force the WNP anomalous cyclone and, consequently, westward extensions (Hong et al., 2014; Lu & Dong, 2005; Zuo et al., 2019). The COMP2 *ATL TBAND* produces a slightly weaker extension compared to COMP1. Since the *ATL EXTBAND* forcings show no significant westward extensions, the difference in the *ATL TBAND* forcings is attributed to the widespread positive tropical North Atlantic SST anomalies in COMP1 that may drive a stronger response over the western North Atlantic.

Unlike the net Pacific forcing of westward extensions, the net forcing from COMP2's Pacific (-16°E) and Atlantic (-17°E) SSTs do not add linearly to recover its original 4xWEST forcing (-21°E) (Figures 4b, 6d, and 8b). The strong relative contributions from both the Pacific and Atlantic basins clearly explain why COMP2 provides a stronger westward extension than COMP1. But, if the two basins provide comparable impacts on the WPSH's westward extension, why does one basin show a stronger forcing over the other? We suggest that, in contemporaneous forcing experiments, the location of the forcing relative to the subsidence region matters. If local and remote SST forcings are similar (as in the case of COMP2), the westward extensions are more likely to be driven by SST anomalies in close proximity to the WPSH. Idealized experiments (not shown) show that the westward extensions are sensitive to zonal shifts of the zonal SST gradient. Studies such as L. Jiang et al. (2023)

JONES ET AL. 11 of 15

21698996, 2024, 15, Downloaded from https://agupubs.onlinelibrary.wiley.com/doi/10.1029/2023JD040429, Wiley Online Library on [27/05/2025]. See the Terms

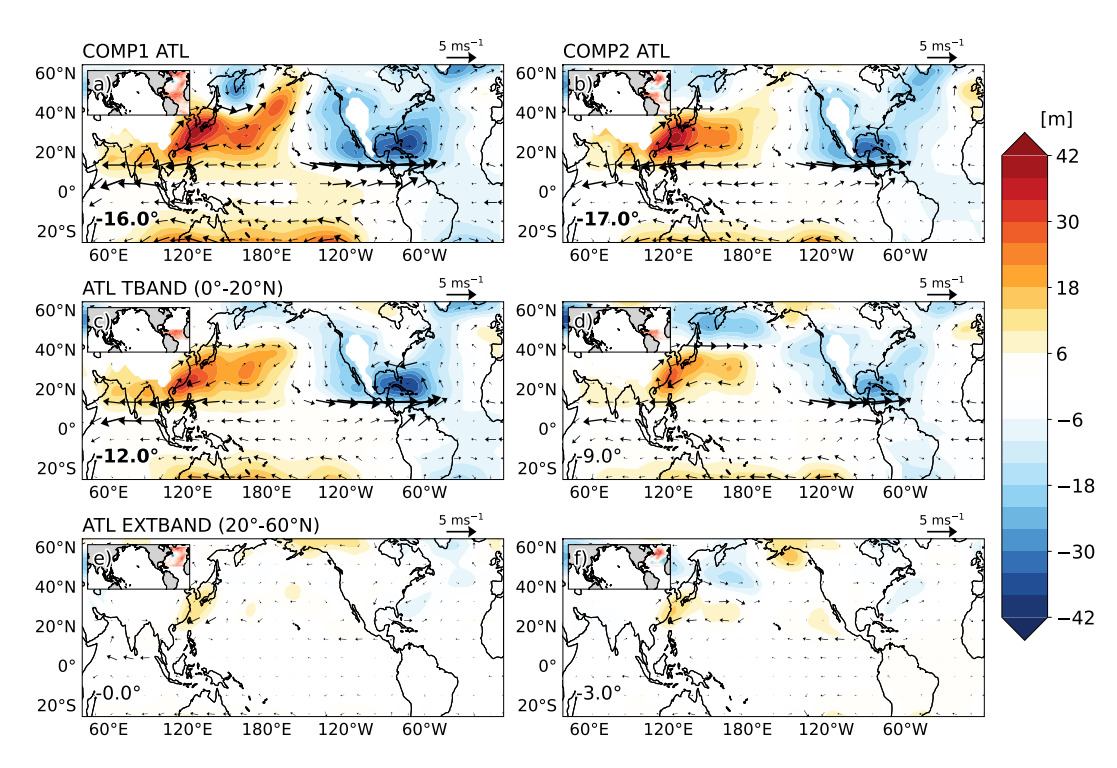


Figure 8. COMP1 versus COMP2 comparison of simulation response to experiments (a, b) *ATL* only, (c, d) *ATL TBAND*, and (e, f) *ATL EXTBAND*.

also imply this sensitivity, as cases in which the westward reach of equatorial Pacific cold SST anomalies (and thus stronger zonal SST gradient) also produce a stronger forcing of WPSH westward extensions.

6. Discussion and Conclusion

Many studies have highlighted the importance of SSTs in driving the WPSH's zonal variability. Many have concluded that the tropical Indian and equatorial eastern Pacific SST variability are key drivers of the WPSH's zonal extensions (H. Li et al., 2020; B. Wang et al., 2013). In this study, we examined which SSTs across the Indian and Pacific Oceans matter for the westward extensions by progressively constraining the SST forcing within atmosphere-only CESM2 model simulations. The simulated WPSH's response to our forcing simulations is outlined in Table 2, and our key conclusions are summarized as follows:

- 1. In comparing two very similar SST patterns (COMP1 and COMP2), we find that the large-scale zonal interbasin SST gradient that characterizes decaying El Niño and developing La Niña summers, is not always the predominant driver of the WPSH's westward extensions. While COMP1 and COMP2 force comparable westward extensions, the relative contributions from remote SSTs (inter-basin forcing) predominantly drive westward extensions in COMP1 simulations, while local Pacific SSTs (intra-basin forcing) are the predominant driver in COMP2 simulations.
- 2. One key reason for the difference in net contributions is likely due to differences in state of the summer El Niño decay. The meridional spread and magnitude of central Pacific and eastern Pacific negative SST anomalies, and even the presence of lingering El Niño-related positive SST anomalies, weakens the Pacific zonal SST gradient in COMP1. However, this only partially explains the inter-basin SST forcing of westward extensions by the COMP1 SST pattern. The second key reason is that the SSTs north of 20°N tend to force anomalous cyclonic circulation over the WNP. In COMP1, the Pacific TBAND forcing of westward extensions is completely suppressed by its PAC EXTBAND forcing, while COMP2's Pacific TBAND forcing is strong enough to withstand suppression from it's PAC EXTBAND forcing.
- 3. When the net *PAC* forcing is weak, the Atlantic SST forcing drives the westward extensions. The COMP1 and COMP2 SST patterns show that a warm *ATL TBAND* forces significant westward extensions. Note that the *PAC* and *ATL* forcing simulations show comparable forcing of westward extensions, but do not contribute in

JONES ET AL. 12 of 15

21698996, 2024, 15, Downloaded from https://agupubs.onlinelibrary.wiley.com/doi/10.1029/2023JD040429, Wiley Online Library on [27/05/2025]. See the Terms and Conditions (https://onlinelibrary.wiley

and-conditions) on Wiley Online Library for rules of use; OA articles are governed by the applicable Creative Commons Licensu

Table 2Summary of the Mean Westward Extension for Each Experiment, Expressed as a Change From the CTRL Simulation

Experiment	COMP1 WEI	COMP2 WEI
4xWEST (Global)	−15°	-21°
4xWEST minus ATL	-2°	-22°
4xWEST minus ATL,TIO	0°	-16°
PAC	1°	-18°
PACx2	− 4°	_
PACx3	− 8°	_
PAC TBAND	−14 °	-19°
PAC EXTBAND	+6°	+8°
ATL only	−16 °	-17°
ATL TBAND	−12 °	-9°
ATL EXTBAND	0°	-3°

Note. Negative (positive) values indicate a westward extension (eastward retraction). As with prior figures, values highlighted in bold represent statistical significance at the 95% confidence level.

equal portions to the original 4xWEST forcing, particularly for COMP2 (see Figure S6 in Supporting Information S1). Instead, they may alternate the driving role of the Walker Circulation, depending on the net Pacific SST forcing, as illustrated by Figure 4. This suggests that the relative contributions of the tropical Indian Ocean, Pacific, and Atlantic basins may be non-linear in nature. This may not be entirely surprising considering that the individual basins can have considerable influence on each other (Chikamoto et al., 2020; Hoerling et al., 2001; Hu & Fedorov, 2020; Park et al., 2023).

The results of this paper also has implications for understanding WPSH westward extension variability and the sources of SST forcing. L. Jiang et al. (2023) showed that the westward extensions are sensitive to the rate of development of ENSO and thus the strength of the tropical zonal SST gradient with negative impacts from subtropical Pacific SSTs. Our study further shows that these characteristics may also determine whether the westward extensions are driven predominantly by inter-basin Atlantic SST forcing versus intra-basin Pacific SST forcing. Additionally, Hong et al. (2014) observed that the influence of tropical Atlantic warming on the WPSH has strengthened in recent over recent decades. Seager et al. (2019) observed that precipitation trends favor increased precipitation over the western Pacific with decreased precipitation over the central Pacific, indicating a strengthening of the zonal equatorial Pacific SST gradient. Further work will examine the contributions

of a warmer tropical Atlantic and strengthened equatorial Pacific SST gradient to future variability and thus predictability of WPSH zonal extensions. Tropical Atlantic warming has been shown to induce a La Niña-like pattern (Chikamoto et al., 2020; Fosu et al., 2020; McGregor et al., 2014; Park et al., 2023). It could be possible in a fully coupled framework, that remote tropical Atlantic warming and the Atlantic's forced development of a La Niña may promote WPSH intensification. In addition, the pattern of Atlantic warming in COMP1 is similar to the positive phase of the Atlantic Multidecadal Variability (AMV) and provides further motivation for understanding of the remote impacts of the Atlantic Ocean on WPSH development.

Data Availability Statement

The SST forcing files and model builds used in this analysis (Jones et al., 2023) are available at the Zenodo repository https://doi.org/10.5281/zenodo.10127842. The ERA5 reanalysis data set (Hersbach et al., 2017) is publicly available through the Copernicus Climate Data Store (https://cds.climate.copernicus.eu). The previous and current versions of the CESM2 global climate model (UCAR, 2018) is freely available to the public and may be found at https://www.cesm.ucar.edu/models/cesm2/.

Acknowledgments References

This research was supported by the

National Science Foundation (NSF)

Faculty Early Career Development

would like to acknowledge high-

performance computing support from

Computational and Information Systems

Cheyenne (https://doi.org/10.5065/D6RX99HX) provided by NCAR's

Laboratory, sponsored by the NSF.

Finally, we thank all the scientists,

software engineers, and administrators

who contributed to the development of

CESM2. We also thank the Editor and

suggestions that helped to improve the quality of our publication.

Reviewers for the helpful comments and

Program (CAREER) Award 1945113. We

Camp, J., Scaife, A. A., & Heming, J. (2018). Predictability of the 2017 North Atlantic hurricane season. Atmospheric Science Letters, 19(5), e813. https://doi.org/10.1002/asl.813

Chaluvadi, R., Varikoden, H., Mujumdar, M., & Ingle, S. (2021). Variability of West Pacific subtropical high and its potential importance to the Indian summer monsoon rainfall. *International Journal of Climatology*, 41(7), 4047–4060. https://doi.org/10.1002/joc.7057

Chang, C., Zhang, Y., & Li, T. (2000). Interannual and interdecadal variations of the East Asian summer monsoon and tropical Pacific SSTs. Part I: Roles of the subtropical ridge. *Journal of Climate*, 13(24), 4310–4325. https://doi.org/10.1175/1520-0442(2000)013%3C4310:IAIVOT% 3E2.0.CO;2

Chen, M., Yu, J.-Y., Wang, X., & Jiang, W. (2019). The changing impact mechanisms of a diverse El Niño on the western Pacific subtropical high. Geophysical Research Letters, 46(2), 953–962. https://doi.org/10.1029/2018GL081131

Chen, P., Hoerling, M. P., & Dole, R. M. (2001). The origin of the subtropical anticyclones. *Journal of the Atmospheric Sciences*, 58(13), 1827–1835. https://doi.org/10.1175/1520-0469(2001)058<1827:tootsa>2.0.co;2

Chen, R., Simpson, I. R., Deser, C., Wang, B., & Du, Y. (2022). Mechanisms behind the springtime north pacific ENSO teleconnection bias in climate models. *Journal of Climate*, 35(23), 4091–4110. https://doi.org/10.1175/JCLI-D-22-0304.1

Chen, W., Park, J.-K., Dong, B., Lu, R., & Jung, W.-S. (2012). The relationship between El Niño and the western north Pacific summer climate in a coupled GCM: Role of the transition of El Niño decaying phases. *Journal of Geophysical Research*, 117(D12). https://doi.org/10.1029/2011D017385

Chen, Z., Wen, Z., Wu, R., Lin, X., & Wang, J. (2016). Relative importance of tropical SST anomalies in maintaining the Western North Pacific anomalous anticyclone during El Niño to La Niña transition years. Climate Dynamics, 46(3–4), 1027–1041. https://doi.org/10.1007/s00382-015-2630-1

JONES ET AL. 13 of 15

- Chikamoto, Y., Johnson, Z. F., Wang, S.-Y. S., McPhaden, M. J., & Mochizuki, T. (2020). El Niño—Southern Oscillation evolution modulated by Atlantic forcing. *Journal of Geophysical Research: Oceans*, 125(8), e2020JC016318. https://doi.org/10.1029/2020JC016318
- Danabasoglu, G., Lamarque, J.-F., Bacmeister, J., Bailey, D., DuVivier, A., Edwards, J., et al. (2020). The community Earth system model version 2 (CESM2). *Journal of Advances in Modeling Earth Systems*, 12(2), e2019MS001916. https://doi.org/10.1029/2019MS001916
- Dong, X., & He, C. (2020). Zonal displacement of the Western North Pacific subtropical high from early to late summer. *International Journal of Climatology*, 40(11), 5029–5041. https://doi.org/10.1002/joc.6508
- Fosu, B., He, J., & Liguori, G. (2020). Equatorial Pacific warming attenuated by SST warming patterns in the tropical Atlantic and Indian Oceans. Geophysical Research Letters, 47(18), e2020GL088231. https://doi.org/10.1029/2020GL088231
- Guan, W., Hu, H., Ren, X., & Yang, X.-Q. (2019). Subseasonal zonal variability of the western Pacific subtropical high in summer: Climate impacts and underlying mechanisms. Climate Dynamics, 53(5), 3325–3344. https://doi.org/10.1007/s00382-019-04705-4
- He, C., & Zhou, T. (2015). Responses of the western North Pacific subtropical high to global warming under RCP4. 5 and RCP8. 5 scenarios projected by 33 CMIP5 models: The dominance of tropical Indian Ocean–tropical western Pacific SST gradient. *Journal of Climate*, 28(1), 365–380. https://doi.org/10.1175/JCLI-D-13-00494.1
- Hersbach, H., Bell, B., Berrisford, P., Biavati, G., Horányi, A., Muñoz Sabater, J., et al. (2017). Complete ERA5 from 1940: Fifth generation of ECMWF atmospheric reanalyses of the global climate [Dataset]. Copernicus Climate Change Service (C3S) Data Store (CDS). https://doi.org/10.24381/cds.143582cf
- Hersbach, H., Bell, B., Berrisford, P., Hirahara, S., Horányi, A., Muñoz Sabater, J., et al. (2020). The ERA5 global reanalysis. *The Quarterly Journal of the Royal Meteorological Society*, 146(730), 1999–2049. https://doi.org/10.1002/qj.3803
- Hoerling, M. P., Hurrell, J. W., & Xu, T. (2001). Tropical origins for recent North Atlantic climate change. Science, 292(5514), 90–92. https://doi.org/10.1126/science.1058582
- Hong, C.-C., Chang, T.-C., & Hsu, H.-H. (2014). Enhanced relationship between the tropical Atlantic SST and the summertime western North Pacific subtropical high after the early 1980s. *Journal of Geophysical Research: Atmospheres*, 119(7), 3715–3722. https://doi.org/10.1002/ 2013JD021394
- Hong, C.-C., Lee, M.-Y., Hsu, H.-H., Lin, N.-H., & Tsuang, B.-J. (2015). Tropical SST forcing on the anomalous WNP subtropical high during July–August 2010 and the record-high SST in the tropical Atlantic. *Climate Dynamics*, 45(3–4), 633–650. https://doi.org/10.1007/s00382-014-2275.5
- Hoskins, B. (1996). On the existence and strength of the summer subtropical anticyclones: Bernhard Haurwitz Memorial Lecture. *Bulletin of the American Meteorological Society*, 77(6), 1287–1292. http://www.jstor.org/stable/26233282
- Hu, S., & Fedorov, A. V. (2020). Indian Ocean warming as a driver of the North Atlantic warming hole. *Nature Communications*, 11(1), 4785. https://doi.org/10.1038/s41467-020-18522-5
- Jiang, L., Chen, H.-C., Li, T., & Chen, L. (2023). Diverse response of Western North Pacific anticyclone to fast-decay El Niño during decaying summer. Geophysical Research Letters, 50(7), e2022GL102612. https://doi.org/10.1029/2022GL102612
- Jiang, W., Huang, P., Wu, R., Hu, K., & Chen, W. (2019). Northwest Pacific anticyclonic anomalies during post–El Niño summers determined by the pace of El Niño decay. *Journal of Climate*, 32(12), 3487–3503. https://doi.org/10.1175/JCLI-D-18-0793.1
- Johnson, Z. F., Chavas, D. R., & Ramsay, H. A. (2022). Statistical framework for western North Pacific tropical cyclone landfall risk through modulation of the western Pacific subtropical high and ENSO. *Journal of Climate*, 35(22), 1–32. https://doi.org/10.1175/JCLI-D-21-0824.1
- Jones, J. J., Chavas, D. R., & Johnson, Z. F. (2023). SST forcing files and Model Builds for "Inter-basin versus intra-basin sea surface temperature forcing of the Western North Pacific subtropical high's westward extensions" [Dataset]. Zenodo. https://doi.org/10.5281/zenodo.10127842
- Jong, B.-T., Ting, M., Seager, R., & Anderson, W. B. (2020). ENSO teleconnections and impacts on US summertime temperature during a multiyear La Niña life cycle. *Journal of Climate*, 33(14), 6009–6024. https://doi.org/10.1175/JCLI-D-19-0701.1
- Kosaka, Y., Xie, S.-P., Lau, N.-C., & Vecchi, G. A. (2013). Origin of seasonal predictability for summer climate over the Northwestern Pacific. Proceedings of the National Academy of Sciences of the United States of America, 110(19), 7574–7579. https://doi.org/10.1073/pnas. 1215582110
- Li, H., Xu, F., & Lin, Y. (2020). The impact of SST on the zonal variability of the western Pacific subtropical high in boreal summer. *Journal of Geophysical Research: Atmospheres*, 125(11), e2019JD031720. https://doi.org/10.1029/2019JD031720
- Li, T., Wang, B., Wu, B., Zhou, T., Chang, C.-P., & Zhang, R. (2017). Theories on formation of an anomalous anticyclone in western North Pacific during El Niño: A review. *Journal of Meteorological Research*, 31(6), 987–1006. https://doi.org/10.1007/s13351-017-7147-6
- Li, W., Li, L., Ting, M., & Liu, Y. (2012). Intensification of Northern Hemisphere subtropical highs in a warming climate. *Nature Geoscience*, 5(11), 830–834. https://doi.org/10.1038/ngeo1590
- Liu, Y., Wu, G., & Ren, R. (2004). Relationship between the subtropical anticyclone and diabatic heating. *Journal of Climate*, 17(4), 682–698. https://doi.org/10.1175/1520-0442(2004)017%3C0682:RBTSAA%3E2.0.CO;2
- Lu, R., & Dong, B. (2001). Westward extension of North Pacific subtropical high in summer. Journal of the Meteorological Society of Japan Series II, 79(6), 1229–1241. https://doi.org/10.2151/jmsj.79.1229
- Lu, R., & Dong, B. (2005). Impact of Atlantic sea surface temperature anomalies on the summer climate in the western North Pacific during 1997–1998. *Journal of Geophysical Research*, 110(D16). https://doi.org/10.1029/2004JD005676
- McGregor, S., Timmermann, A., Stuecker, M. F., England, M. H., Merrifield, M., Jin, F.-F., & Chikamoto, Y. (2014). Recent Walker circulation strengthening and Pacific cooling amplified by Atlantic warming. *Nature Climate Change*, 4(10), 888–892. https://doi.org/10.1038/nclimate2330
- Miyasaka, T., & Nakamura, H. (2005). Structure and formation mechanisms of the Northern Hemisphere summertime subtropical highs. *Journal of Climate*, 18(23), 5046–5065. https://doi.org/10.1175/JCLI3599.1
- Park, J.-H., Yeh, S.-W., Kug, J.-S., Yang, Y.-M., Jo, H.-S., Kim, H.-J., & An, S.-I. (2023). Two regimes of inter-basin interactions between the Atlantic and Pacific Oceans on interannual timescales. npj Climate and Atmospheric Science, 6(1), 13. https://doi.org/10.1038/s41612-023-00332-3
- Qian, W., & Shi, J. (2017). Tripole precipitation pattern and SST variations linked with extreme zonal activities of the western Pacific subtropical high. *International Journal of Climatology*, 37(6), 3018–3035. https://doi.org/10.1002/joc.4897
- Rodwell, M. J., & Hoskins, B. J. (2001). Subtropical anticyclones and summer monsoons. *Journal of Climate*, 14(15), 3192–3211. https://doi.org/10.1175/1520-0442(2001)014%3C3192:SAASM%3E2.0.CO;2
- Rong, X., Zhang, R., & Li, T. (2010). Impacts of Atlantic sea surface temperature anomalies on Indo-East Asian summer monsoon-ENSO relationship. Chinese Science Bulletin, 55(22), 2458–2468. https://doi.org/10.1007/s11434-010-3098-3
- Seager, R., Cane, M., Henderson, N., Lee, D.-E., Abernathey, R., & Zhang, H. (2019). Strengthening tropical Pacific zonal sea surface temperature gradient consistent with rising greenhouse gases. *Nature Climate Change*, 9(7), 517–522. https://doi.org/10.1038/s41558-019-0505-x

JONES ET AL. 14 of 15



Journal of Geophysical Research: Atmospheres

- 10.1029/2023JD040429
- Seager, R., Murtugudde, R., Naik, N., Clement, A., Gordon, N., & Miller, J. (2003). Air-sea interaction and the seasonal cycle of the subtropical anticyclones. *Journal of Climate*, 16(12), 1948–1966. https://doi.org/10.1175/1520-0442(2003)016<1948:AIATSC>2.0.CO:2
- Stuecker, M. F., Jin, F.-F., Timmermann, A., & McGregor, S. (2015). Combination mode dynamics of the anomalous northwest Pacific anti-cyclone. *Journal of Climate*, 28(3), 1093–1111. https://doi.org/10.1175/JCLI-D-14-00225.1
- UCAR. (2018). Community Earth system model (version 2.0) [Software]. University Corporation for Atmospheric Research. Retrieved from https://www.cesm.ucar.edu/models/cesm2/
- Wang, B., Wu, R., & Li, T. (2003). Atmosphere-warm ocean interaction and its impacts on Asian–Australian monsoon variation. *Journal of Climate*, 16(8), 1195–1211. https://doi.org/10.1175/1520-0442(2003)16%3C1195:AOIAII%3E2.0.CO;2
- Wang, B., Xiang, B., & Lee, J.-Y. (2013). Subtropical high predictability establishes a promising way for monsoon and tropical storm predictions. *Proceedings of the National Academy of Sciences of the United States of America*, 110(8), 2718–2722. https://doi.org/10.1073/pnas.
- Wang, X., Li, T., & He, C. (2021). Impact of the mean state on El Niño-Induced Western North Pacific anomalous anticyclones during El Niño decaying summer in AMIP models. *Journal of Climate*, 34(22), 9201–9217. https://doi.org/10.1175/JCLI-D-20-0747.1
- Williams, I. N., & Patricola, C. M. (2018). Diversity of ENSO events unified by convective threshold sea surface temperature: A nonlinear ENSO index. Geophysical Research Letters, 45(17), 9236–9244. https://doi.org/10.1029/2018GL079203
- Wu, B., Li, T., & Zhou, T. (2010). Relative contributions of the Indian ocean and local SST anomalies to the maintenance of the Western North Pacific anomalous anticyclone during the El Niño decaying summer. *Journal of Climate*, 23(11), 2974–2986. https://doi.org/10.1175/ 2010ICLJ3300.1
- Wu, B., Zhou, T., & Li, T. (2009). Seasonally evolving dominant interannual variability modes of east Asian climate. *Journal of Climate*, 22(11), 2992–3005. https://doi.org/10.1175/2008JCLI2710.1
- Wu, L., & Wang, C. (2015). Has the western Pacific subtropical high extended westward since the late 1970s? *Journal of Climate*, 28(13), 5406–5413. https://doi.org/10.1175/JCLI-D-14-00618.1
- Wu, M., Zhou, T., & Chen, X. (2021). The source of uncertainty in projecting the anomalous western North Pacific anticyclone during El Niñodecaying summers. *Journal of Climate*, 34(16), 6603–6617. https://doi.org/10.1175/JCLI-D-20-0904.1
- Wu, M., Zhou, T., Chen, X., & Wu, B. (2020a). Intermodel uncertainty in the projection of the anomalous western North Pacific anticyclone associated with El Niño under global warming. *Geophysical Research Letters*, 47(2), e2019GL086139. https://doi.org/10.1029/2019GL086139
- Wu, Q., Wang, X., & Tao, L. (2020b). Interannual and interdecadal impact of Western North Pacific subtropical high on tropical cyclone activity. Climate Dynamics, 54(3), 2237–2248. https://doi.org/10.1007/s00382-019-05110-7
- Xie, S.-P., Hu, K., Hafner, J., Tokinaga, H., Du, Y., Huang, G., & Sampe, T. (2009). Indian Ocean capacitor effect on Indo-western Pacific climate during the summer following El Niño. *Journal of Climate*, 22(3), 730–747. https://doi.org/10.1175/2008JCL12544.1
- Yan-Yan, H., & Xiao-Fan, L. (2015). The interdecadal variation of the western pacific subtropical high as measured by 500 hpa eddy geopotential height. Atmospheric and Oceanic Science Letters, 8(6), 371–375. https://doi.org/10.3878/AOSL20150038
- Yimin, L., & Guoxiong, W. (2004). Progress in the study on the formation of the summertime subtropical anticyclone. *Advances in Atmospheric Sciences*, 21(3), 322–342. https://doi.org/10.1007/bf02915562
- Zhou, T., Yu, R., Zhang, J., Drange, H., Cassou, C., Deser, C., et al. (2009). Why the western Pacific subtropical high has extended westward since the late 1970s. *Journal of Climate*, 22(8), 2199–2215. https://doi.org/10.1175/2008JCLI2527.1
- Zuo, J., Li, W., Sun, C., & Ren, H.-C. (2019). Remote forcing of the northern tropical Atlantic SST anomalies on the western North Pacific anomalous anticyclone. Climate Dynamics, 52(5–6), 2837–2853. https://doi.org/10.1007/s00382-018-4298-9

JONES ET AL. 15 of 15